MATERIALS SCIENCE

Thin films of topological Kondo insulator candidate SmB_6: Strong spin-orbit torque without exclusive surface conduction

Yufan Li,* Qinli Ma, S. X. Huang,† C. L. Chien*

The advent of topological insulators (TIs), a novel class of materials that harbor a metallic spin-chiral surface state coexisting with band-insulating bulk, opens up new possibilities for spintronics. One promising route is current-induced switching of an adjacent magnetic layer via spin-orbit torque (SOT), arising from the large spin-orbit coupling intrinsically possessed by TIs. The Kondo insulator SmB_6 has been recently proposed to be a strongly correlated TI, supported by the observation of a metallic surface state in bulk SmB_6, as evidenced by the thickness independence of the low-temperature resistance plateau. We report the synthesis of epitaxial (001) SmB_6/Si thin films and a systematic thickness-dependent electrical transport study. Although the low-temperature resistance plateau is observed for all films from 50 to 500 nm in thickness, the resistance is distinctively thickness-dependent and does not support the notion of surface conduction and interior insulation. On the other hand, we demonstrate that SmB_6 can generate a large SOT to switch an adjacent ferromagnetic layer, even at room temperature. The effective SOT generated from SmB_6 is comparable to that from β-W, one of the strongest SOT materials.

INTRODUCTION

The strong spin-orbit coupling (SOC) of topological insulators (TIs) manifests itself in exotic ways, such as the spin-chiral surface state (*1*). The locking between the momentum and the spin of carriers on the surface state, together with the SOC, may lead to new applications in spintronics (*2*). It has been shown that the TIs have giant spin Hall angles (*3*) and that the chiral spin-momentum locking can be observed by electrical transport measurements (*4*–*6*). However, despite the intense experimental effort waged on the traditional Bi-based TIs, such as Bi_2Se_3, demonstrations of applicable devices are few. A promising pathway toward applications is to use the current-induced spin-orbit torque (SOT) originated from SOC. Such a paradigm has been established in heavy metal (HM) ferromagnet (FM) heterostructures, where the strong SOT generated from the HM can switch the magnetization of the adjacent FM layer (*7*, *8*). Similar experiments have been demonstrated for TI/Cr-doped TI heterostructures at 2 K, where TI replaces the HM and the Cr-doped TI replaces the FM (*9*). However, fully switching of an FM at room temperature via TI has remained elusive until very recently (*10*, *11*).

It may be beneficial to explore new TIs beyond the traditional bismuth chalcogenides. A hopeful candidate is SmB_6, a prototype Kondo insulator known for exhibiting an exotic ground state, where a sudden quenching of the *f*-electron magnetic moment is accompanied by the *d*-*f* band hybridization and the opening of a narrow band gap. It was recently proposed that the strong SOC associated with *d*-*f* hybridization could give rise to a topologically nontrivial surface state (*12*, *13*). SmB_6 and other Kondo insulators have been predicted to be a new class of strongly correlated TIs, that is, topological Kondo insulators (TKIs) (*14*–*16*). SmB_6 is known to show a highly unusual saturation of low-temperature resistivity, instead of diverging, despite the presence of a hybridization gap (*17*, *18*). In light of the TKI theory, the long-standing mystery might be elegantly accounted for as the dominance of the surface conduction when the bulk conduction vanishes, and henceforth be regarded as the key signature of the topological surface state (TSS) of TI. This transport feature would indicate that SmB_6 may have both an insulating interior and a metallic surface (*19*–*21*), features that have eluded the traditional Bi-based TIs, which unfortunately display significant bulk conduction with very few exceptions (*22*, *23*).

However, experiments set out to verify the topological nature of SmB_6 reached contradicting verdicts. The in-gap states with apparent linear dispersion, which could be interpreted as the TSS, were observed by angle-resolved photoemission spectroscopy (ARPES) (*24*–*29*). One specific study further observed spin-momentum locking, a key feature of TSS (*29*). However, the Dirac point of the TSS was never identified by ARPES, leaving room to ascribe the observed in-gap state to other topologically trivial origins, such as the Rashba effect (*27*, *30*). Quantum oscillations revealed by torque magnetometry were once believed to evidence two-dimensional (2D) Fermi surfaces as a strong support to the presence of TSS (*31*), but it is now argued by a similar study that the oscillations are completely of bulk origin (*32*). On the other hand, results from the electrical transport studies of bulk crystals consistently conclude the presence of a metallic surface state with one accord (*19*–*21*, *33*–*35*). Most notably, Kim *et al.* (*21*) reported that the low-temperature saturation plateau value of resistance is independent of the thickness of the bulk crystals, whereas the resistance plateau itself is vulnerable to magnetic impurity doping, consistent with the predicted topological nature of TSS.

Most studies to date use bulk crystals or thin slabs with thicknesses in the 100-μm range. Conspicuously lacking are epitaxial thin films, which provide the necessary sensitivity to address the conducting characteristics of the interior. High-quality thin films, once available, open paths to applications such as SOT-induced switching, which may exploit the topological nature in question.

Here, we investigate the correlation, if any, between the low-temperature resistance plateau and the presence of a metallic surface state in (001) SmB_6/Si thin films with dominant epitaxy as grown by dc magnetron sputtering. We systematically study the thickness dependence of the transport properties. Our results show that although thin films manifest a low-temperature resistance plateau along with

Department of Physics and Astronomy, Johns Hopkins University, Baltimore, MD 21218, USA.
*Corresponding author. Email: yli171@pha.jhu.edu (Y.L.); clchien@jhu.edu (C.L.C.)
†Present address: Department of Physics, University of Miami, Coral Gables, FL 33146, USA.

an insulating phase (consistent with the observations in bulk samples), the resistance shows unequivocal thickness dependence, contradicting the notion of 2D surface conduction. On the other hand, SmB_6 thin films host strong SOT that induces magnetic switching of an adjacent CoFeB or Co layer with perpendicular magnetic anisotropy (PMA), even at room temperature.

RESULTS

Thin-film characterization and the lack of 2D surface transport signature

We fabricated (001) SmB_6 films by dc magnetron sputtering from a single SmB_6 target in a high vacuum chamber (base pressure, 3×10^{-8} torr) on HF-etched undoped Si(001) substrates at a substrate temperature of 550°C, with a −90 V bias applied between the sample and the electrical ground. The biased sputtering helps to stabilize rare-earth hexaborides growth and to achieve stoichiometry (*36*). The choice of the Si(001) substrate is based on the cubic crystal structure of SmB_6, with a lattice parameter of 4.13 Å as shown in Fig. 1A, where a cube of 8 Sm atoms encloses an octahedron of B atoms. The SmB_6(100) plane, after a 45° rotation, matches closely with the Si(100) of Si (lattice parameter of 3.84 Å), with a 7% lattice mismatch (that is, with the epitaxy relationship of SmB_6[100] ∥ Si[110]). The x-ray diffraction (XRD) pattern shown in Fig. 1B measures the out-of-plane lattice constant and indicates only the (001) SmB_6 phase. Furthermore, SmB_6/Si(001) films display a dominant epitaxy relationship of SmB_6(100) ∥ Si[110] as revealed by XRD ϕ scan, as shown in Fig. 1C. A comparative x-ray photoelectron spectroscopy (XPS) measurement (shown in the Supplementary Materials) confirms the correct Sm/B stoichiometry. We patterned SmB_6 films (50 to 500 nm in thickness) into Hall bars for transport measurements.

For thin films, it is useful to express transport properties as sheet resistance ($R_\square = R \cdot W/L = \rho/d$) and sheet conductance ($G_\square = R_\square^{-1}$), where W, L, and d are the width, length, and thickness, respectively, of a thin film of resistance R and resistivity ρ. Figure 1D shows a temperature-dependent $R_\square$ of our SmB_6/Si(001) thin film (250 nm in thickness as a representative example). Overall, it demonstrates a similar behavior as those in bulk single-crystal samples (*19*, *21*). In particular, $R_\square$ increases as temperature decreases and reaches a plateau at about 10 K. We model the measured conductance as two conductors in parallel, that is, $G_{measured} = G_{plateau} + G_{insulator}$, following the study of Wolgast *et al.* (*19*). Because $G_{insulator}$ is the conductance of the insulating phase that resulted from the *d-f* hybridization gap, it is therefore described by the Arrhenius equation $G_{insulator} = G_a \exp(-\Delta/k_B T)$. The inset in Fig. 1D shows the Arrhenius plot of ln $G_{insulator}$ versus $1/T$; the activation energy Δ can be extracted from the slope. As shown in Fig. 1E, the values of Δ obtained from thin films of various thicknesses consistently give 3.0 ± 0.2 meV, in good agreement with the values of 2.7 to 3.5 meV from bulk samples (*18*, *19*, *35*), as marked by the dashed lines. These results indicate that the gaps in the film samples are electrically as insulating as those in single-crystal bulk samples.

We now discuss the difference between our thin-film samples (50 to 500 nm) and the bulk samples (100 to 1000 μm) from previous studies. In bulk SmB_6, the resistance undergoes a marked increase once the hybridization gap is opened. The saturation resistance at low temperatures is usually 10^3 to 10^5 times higher than that at room temperature (*17*–*19*, *21*, *34*). The saturation resistance appears to be insensitive to thickness, albeit in the 100-μm range (*21*), as might be expected for a 2D surface state. Others report that the ratio of resistance decreases as the sample thickness is reduced (*17*, *35*) because of the competition between the 2D surface conduction and the 3D bulk conduction (*35*). In contrast, the behaviors in thin films—three orders of magnitude thinner—are markedly different. In thin films, the resistance also increases but only by a factor of 2 (*37*) or 30% as in this work. One possible reason is the dominance of the surface conduction over the bulk contribution, which is greatly suppressed in thin films. In the study of Yong *et al.* (*37*), the reduced resistance ratio was considered as evidence for the presence of a 2D surface conduction.

However, should a 2D surface conducting state exist, it can best be revealed from the thickness dependence in thin films. In Fig. 2A, we plot

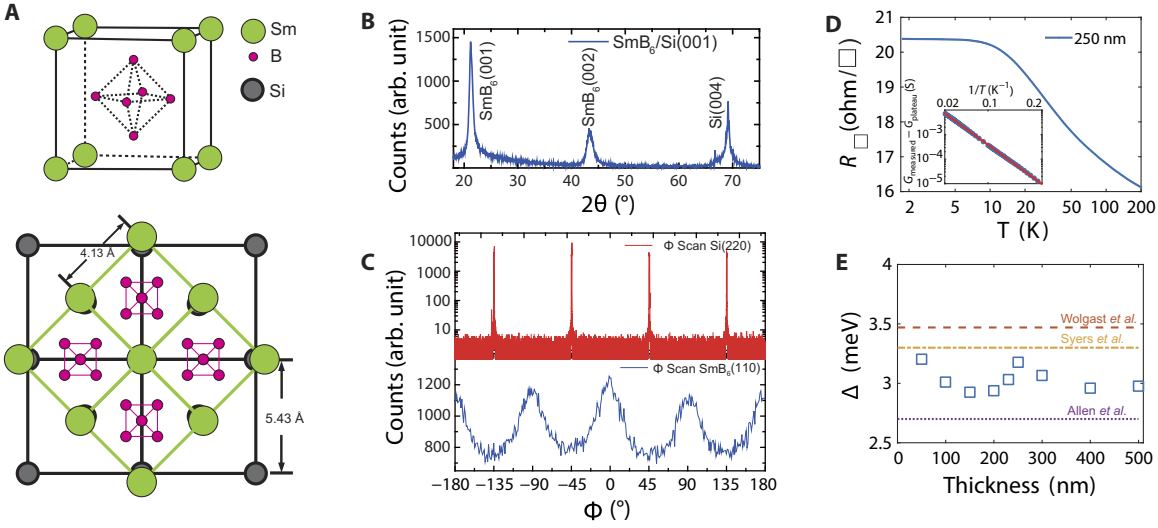

Fig. 1. Crystal structure characterization and transport properties of SmB_6 thin films. (**A**) Crystal structure of SmB_6 (top) and epitaxy relation of SmB_6/Si(001). (**B**) Out-of-plane θ/2θ XRD of the 250-nm-thick SmB_6/Si(001) film. (**C**) In-plane ϕ scan of the Si(220) peak (top) and the SmB_6(110) peak (bottom). (**D**) Temperature dependence of the sheet resistance for the 250-nm-thick film of SmB_6/Si(001). Inset: Representative Arrhenius plot of $G_{measured} - G_{plateau}$ as a function of $1/T$ for the 250-nm-thick film, from 50 to 5 K. The red curve shows the linear fitting of ln $G_{insulator}$ versus $1/T$. (**E**) Activation energy Δ derived from the Arrhenius plot for various film thicknesses. The dashed lines denote Δ values reported in previous bulk SmB_6 studies (*18*, *19*, *35*).

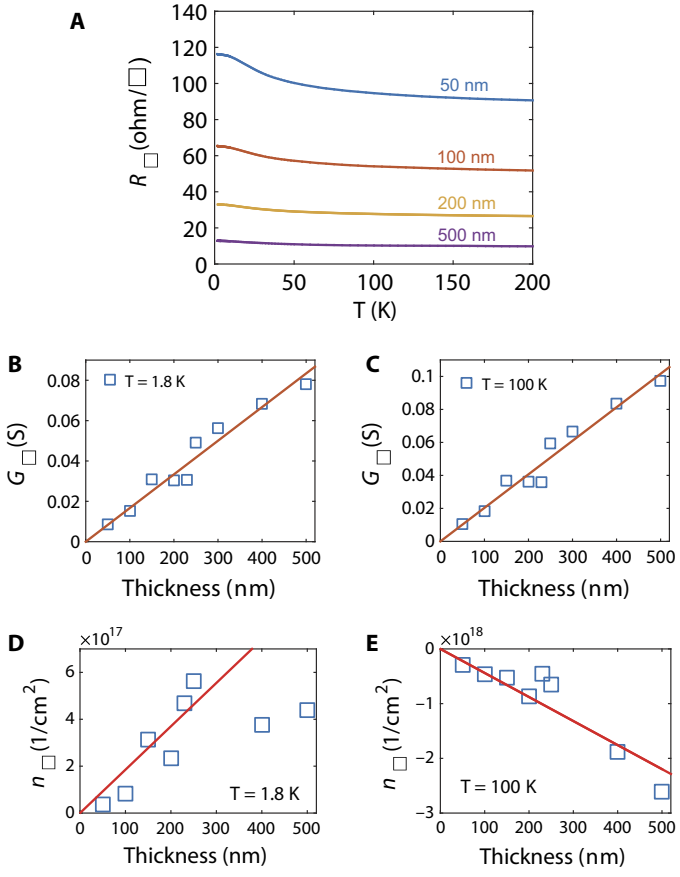

Fig. 2. Thickness dependence of sheet resistance and sheet carrier density. (**A**) Sheet resistance for SmB_6 films with various thicknesses as a function of temperature. Thickness dependence of the sheet conduction of SmB_6 thin films at 1.8 K (**B**) and 100 K (**C**). Thickness dependence of the sheet carrier concentration $n_\square$ at 1.8 K (**D**) and 100 K (**E**).

$R_\square$ as a function of temperature for several representative thicknesses, from 50 to 500 nm. Throughout the entire temperature range (1.8 to 200 K), $R_\square$ exhibits a strong thickness dependence, contrary to the expectation of a 2D surface state, for which plateau $R_\square$ at the low temperature should be thickness-independent to reflect the signature of 2D transport (*21*). In Fig. 2 (B and C), we plot the sheet conductance ($G_\square$) as a function of the film thickness, measured at 1.8 and 100 K, respectively, to distinguish the 2D and 3D transport feature in a quantitative way. As inferred from the results on bulk SmB_6, the low-temperature resistance plateau indicates the dominance of a 2D surface conduction, that is, $G_\square$ remains a constant regardless of film thickness; at higher temperature (for example, 100 K), where the hybridization gap is deemed to close, the material should instead behave as a conventional 3D conductor, that is, $G_\square = \sigma_{xx}d$, a product of longitudinal conductivity σ_{xx} and the film thickness d. At 100 K, $G_\square$ is linearly proportional to d, consistent with a 3D conductor as described by Ohm's law, as shown in Fig. 2C. However, at 1.8 K (as shown in Fig. 2B), $G_\square$ remains linearly proportional to d, showing no deviation from Ohm's law. That is, despite tantalizing suggestions from bulk samples, SmB_6 thin films exhibit no clear evidence of a TI, where the interior is insulating with only the surface metallic state. From the thickness dependence of the Hall effect, one reaches the same conclusion. In Fig. 2 (D and E), we show the sheet carrier density $n_\square$ (the number of carriers per unit square) obtained from the Hall effect measurement, as a function of thickness, for two representative temperatures (1.8 and 100 K). Similar to the analysis of $G_\square$, $n_\square$ is expected to be proportional to the thickness for a 3D conductor, but a constant for a 2D conductor.

Our findings pose fundamental questions on the current understanding of SmB_6. Many studies on bulk SmB_6 indicate or imply that the low-temperature plateau is a manifestation of, topological or not, the surface conductance. The plateau itself would often serve as an evidence for the surface state (*37*, *38*). Thin films would be far more sensitive than bulk crystals to reveal the surface states. Our results show, for thin films on the 100-nm scale, that although the low-temperature plateau is present (albeit reduced in scale), there are no telltale thickness independence conduction characteristics necessary to confirm the 2D surface conduction. In contrast, the thin-film results point to a seemingly 3D origin. It raises the question of the role and nature of the low-temperature plateau and its connection with 2D surface conduction, if any.

SOT-induced switching of the PMA FM layer via SmB_6 thin films

The fact that SmB_6 thin films do not provide evidence of an exclusive surface conduction channel does not necessarily affect its topological nature or the lack thereof. A similar situation occurs in Bi_2Se_3, the well-known TI, whose interior also consistently fails to be insulating, but the topological properties including the novel surface states remain viable. To gain more insight into the case of SmB_6, we have exploited the SOT-induced switching via the SmB_6 thin films.

We used the composite trilayer structure MgO(1.5)/CFB(1)/β-W (0.8), where CFB denotes a well-known ferromagnetic $Co_{40}Fe_{40}B_{20}$ and the numbers in parentheses are thicknesses in nanometers. This is a well-known trilayer structure, in which the CFB layer acquires PMA when sandwiched between MgO and β-W (*39*). The β-W thickness is kept at a minimum to achieve PMA. The trilayer was deposited on SmB_6/Si(001) films of several SmB_6 thicknesses, and the multilayer films were patterned into 20-μm-wide Hall bar devices for transport measurements. The trilayers without SmB_6 were also patterned and measured.

The PMA of the CFB and switching by a perpendicular magnetic field can be evidenced by the anomalous Hall effect (AHE), as shown in Fig. 3B. The blue curve shows the results for the trilayer without SmB_6. When the trilayer is deposited on SmB_6 films, the shunting effect through the more conductive SmB_6 layer reduces the current through the CFB layer, thereby reducing the magnitude of the AHE signal. With an additional SmB_6(50) layer of 50 nm, using the conductors-in-parallel model, one finds the ratio of $I_{SmB_6}/I_{CFB} \approx 13$, determined from the reduced resistance of the Hall bar.

The AHE signal in the trilayer deposited on SmB_6 films also allows the determination of current distribution in the trilayer and the SmB_6 layer. With an additional SmB_6 layer, the greatly reduced AHE resistance R_H has been multiplied 150 times (the red curve) to be comparable to the blue curve in Fig. 3B. The SmB_6(50) layer reduces the R_H value by about 180 times. The current shunting effect of the SmB_6(50) layer in AHE dilutes the current through the CFB layer, and again dilutes the AHE voltage that originates from the CFB layer. Thus, the AHE measurements give the ratio of $I_{tot}/I_{trilayer} \approx (180)^{1/2} \approx 13$, in excellent agreement with resistance measurements. In both cases, most of the current flows through the SmB_6(50) layer with $I_{SmB_6}/I_{tot} \approx 92\%$. More details of the analysis on current distribution can be found in section S5. Figure 3C shows the current distribution in the SmB_6 layers for various layer thicknesses, derived from both the shunting effect of AHE

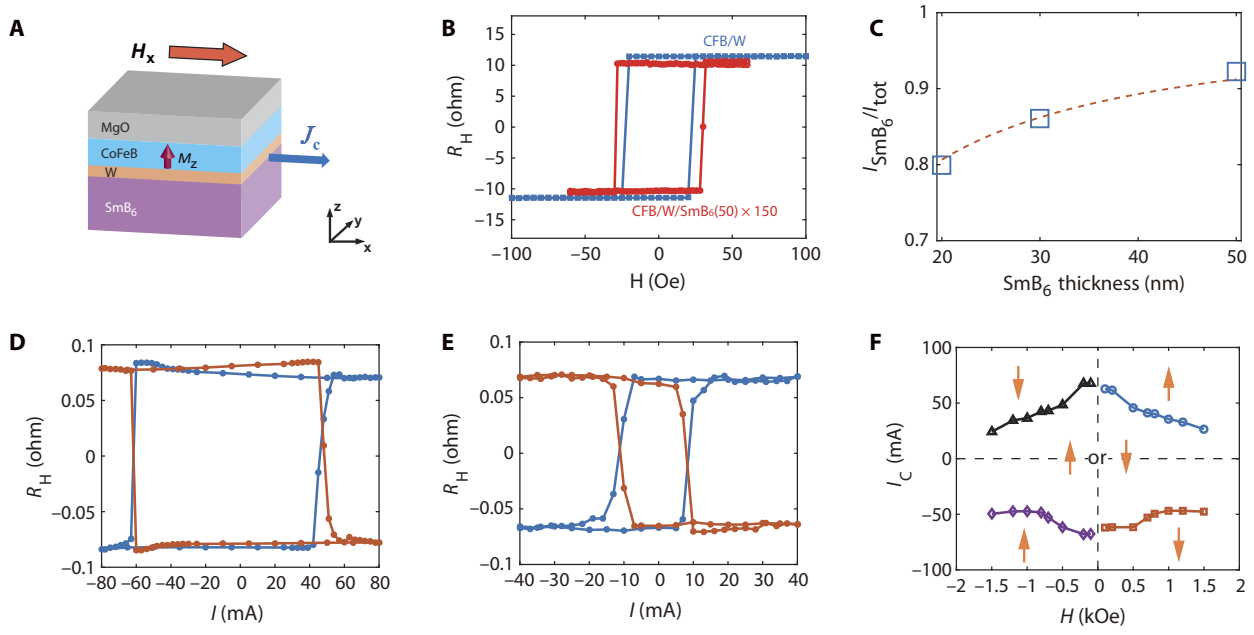

Fig. 3. SOT-induced switching of CFB/W/SmB_6 devices. (**A**) Schematic drawing of the device for SOT-induced switching experiment. (**B**) Hall resistance for the trilayer MgO(1.5)/CFB(1)/W(0.8) (blue) and MgO(1.5)/CFB(1)/W(0.8)/SmB_6(50) (red). The latter is magnified 150 times. (**C**) Current distribution in SmB_6 of CFB/W/SmB_6 multilayers for various SmB_6 film thicknesses. The red dashed line shows the calculation using longitudinal resistivity. SOT switching for CFB(1)/W(0.8)/SmB_6(50) measured at 20 K (**D**) and 300 K (**E**), with external magnetic fields of 500 Oe (blue) and −500 Oe (red) applied along the *x* direction. (**F**) Switching phase diagram of CFB(1)/W(0.8)/SmB_6(50) at 20 K.

and the conductors-in-parallel model based on resistance. Because of the higher conductance of the SmB_6 layer, the current that flows therein (I_{SmB_6}) takes a major fraction of the total applied current (I_{tot}).

The current flowing through the device also exerts the SOT to the magnetic moments in the FM layer, which, together with an applied in-plane magnetic field along the current direction, induces switching of perpendicular magnetic moments (*7*, *8*). The experimental result of these switchings is shown in Fig. 3 (D and E) for the device with the SmB_6(50) layer, performed at 20 and 300 K, respectively. The critical switching current I_C translates to nominal critical current density of 5.2×10^6 A/cm^2 and 8.6×10^5 A/cm^2, respectively. An in-plane magnetic field (500 Oe) is applied along the current direction, which determines the polarity of switching, consistent with the SOT-induced switching in HM/FM heterostructures. In Fig. 3F, we plot a representative phase diagram of the magnetization state, where the astroid-shaped switching polarity can be observed, similar to the case of HM/FM heterostructures. In particular, the switching parity $[(+H_x, +I) \rightarrow +M_z]$ is similar to HMs with a negative spin Hall angle, such as Ta and W.

It is known that β-W is a source of strong SOT by itself (*39*, *40*). In our case, although the thickness of the β-W layer is kept at a minimum to obtain PMA, the SOT generated from β-W would induce switching when a sufficiently large current is applied. Therefore, to clarify the origin of the observed SOT in our trilayers with SmB_6, one needs to compare the I_C with that of the trilayers without SmB_6. In Fig. 4A, we plot I_C for the trilayer with and without SmB_6(50). Should SmB_6(50) in the former contribute no SOT at all but only dilute the current flowing in W, I_C would be enlarged by a factor of $(1\text{-}I_{SmB_6}/I_{tot})^{-1} \approx 13$, compared to that without SmB_6 (Fig. 4A, dashed line). In contrast, the actual I_C with SmB_6(50) is only about 50 mA for 20 K and 10 mA for 300 K, that is, only about half of the presumed value, indicating that SmB_6(50) contributes one-half of the SOT required to switch the magnetization of CFB. The ratio of SOT contributed by SmB_6, $r_{SOT} \equiv SOT_{SmB_6}/SOT_{tot}$, can be quantified as $[I_C^{trilayer} - I_C^{SmB_6} \times (1 - I_{SmB_6}/I_{tot})]/I_C^{trilayer}$. In Fig. 4B, we plot SOT_{SmB_6}/SOT_{tot} for SmB_6 film thicknesses of 20, 30, and 50 nm. The contribution from SmB_6 monotonically increases with increasing film thickness, confirming that SmB_6 is the source of the SOT.

Despite the difficulty presented by the inevitable presence of the β-W buffer layer, which is essential for establishing PMA in CFB, we now estimate the SOT contributed by SmB_6 in a semiquantitative approach, that is, to compare its strength with that of β-W. The spin current generated by SmB_6 transverses into the CFB layer through the W buffer layer, within which it decays by a factor of e^{-t_W/λ_W}, where t_W is the thickness of W and λ_W is the spin diffusion length of W. One can therefore calculate the SOT from SmB_6, should the CFB layer be in direct contact with it, that is, without spin current decay when transferred through the intervening layer. Hence, the efficiency of SmB_6 as an SOT generator can be compared with that of β-W, by comparing the critical current density J_c for switching the same CFB layer with the aid of the same in-plane field. Figure 4C shows J_c for 0.8- and 5-nm-thick β-W and estimated J_c for 50-nm-thick SmB_6, calculated as $J_c^{SmB_6} = I_c \times e^{-t_W/\lambda_W}/(r_{SOT} \times s)$, where *s* is the area of the cross section of the SmB_6 layer and λ_W is taken as 1.5 nm (*41*). In terms of generating SOT, 50-nm-thick SmB_6 is much more effective than 0.8-nm-thick β-W, but is comparable to 5-nm-thick β-W.

The above conclusion of SmB_6 delivering substantial SOT is based on analyses of the current distribution within the multilayers. We use an alternative approach to directly reveal the strong SOT from SmB_6. We note that, in Pt/Co/Pt, the 0.5-nm-thick Co layer sandwiched between two Pt layers of 1.7 nm (top) and 2 nm (bottom) exhibits PMA. The switching parity ($[(+H_x, +I) \rightarrow -M_z]$) of devices made of the Pt/Co/Pt trilayer reveals a positive spin Hall angle, as expected from Pt. We then patterned devices of Pt/Co/Pt/SmB_6, the same Pt/Co/Pt structure on 50 nm of SmB_6. Now, the switching parity of Pt/Co/Pt/SmB_6 shows a negative spin Hall angle. This result conclusively shows that SmB_6 has a

negative spin Hall angle and that the large SOT from SmB_6 can overtake the SOT from Pt of the opposite sign. These results have been observed at the representative temperatures of 20 and 300 K, as shown in Fig. 5 (A to D), and the temperatures in between.

The nominal critical switching current density $|J_c|$ for both samples is summarized in Fig. 5E. The competing spin currents generated from the top and bottom Pt layers result in relatively high $|J_c|$ for the Pt/Co trilayer, although the contribution from the thicker bottom Pt layer prevails, which dictates a Pt-like switching parity. The SOT switching in the Pt/Co/Pt/SmB_6 device occurs despite the fact that the Pt/Co/Pt trilayer is much more conductive than the MgO/CFB/W trilayer and diverts about one-third of the total current as opposed to 8% in the latter case.

Once we take into account the current distribution in SmB_6 and the Pt/Co trilayer, and the opposing SOT generated by the trilayer itself, the critical current density required in the SmB_6 layer is further reduced to 1×10^{-6} A/cm^2 to 3×10^{-6} A/cm^2, which would generate sufficient SOT to switch the FM trilayer. The result is summarized in Fig. 5F.

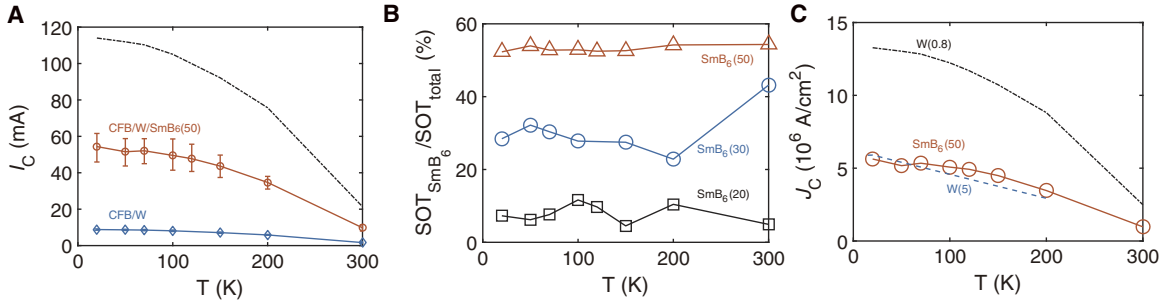

Fig. 4. The SOT originated from the SmB_6 film and its relative strength. (**A**) Critical switching current I_C for MgO(1.5)/CFB(1)/W(0.8)/SmB_6(50) ($I_C^{SmB_6}$, red) and the trilayer MgO(1.5)/CFB(1)/W(0.8) ($I_C^{trilayer}$, blue), and the estimated I_C for MgO(1.5)/CFB(1)/W(0.8)/SmB_6(50) assuming that SmB_6 only dilutes the current (black). (**B**) Percentage of SOT contributed by the SmB_6 layer of MgO(1.5)/CFB(1)/W(0.8)/SmB_6(*t*), where the thickness of SmB_6 *t* takes 20 nm (black), 30 nm (blue), and 50 nm (red). (**C**) Critical current density of 0.8-nm W (purple), 5-nm W (black), and 50-nm SmB_6 for switching a CFB layer if in direct contact with them.

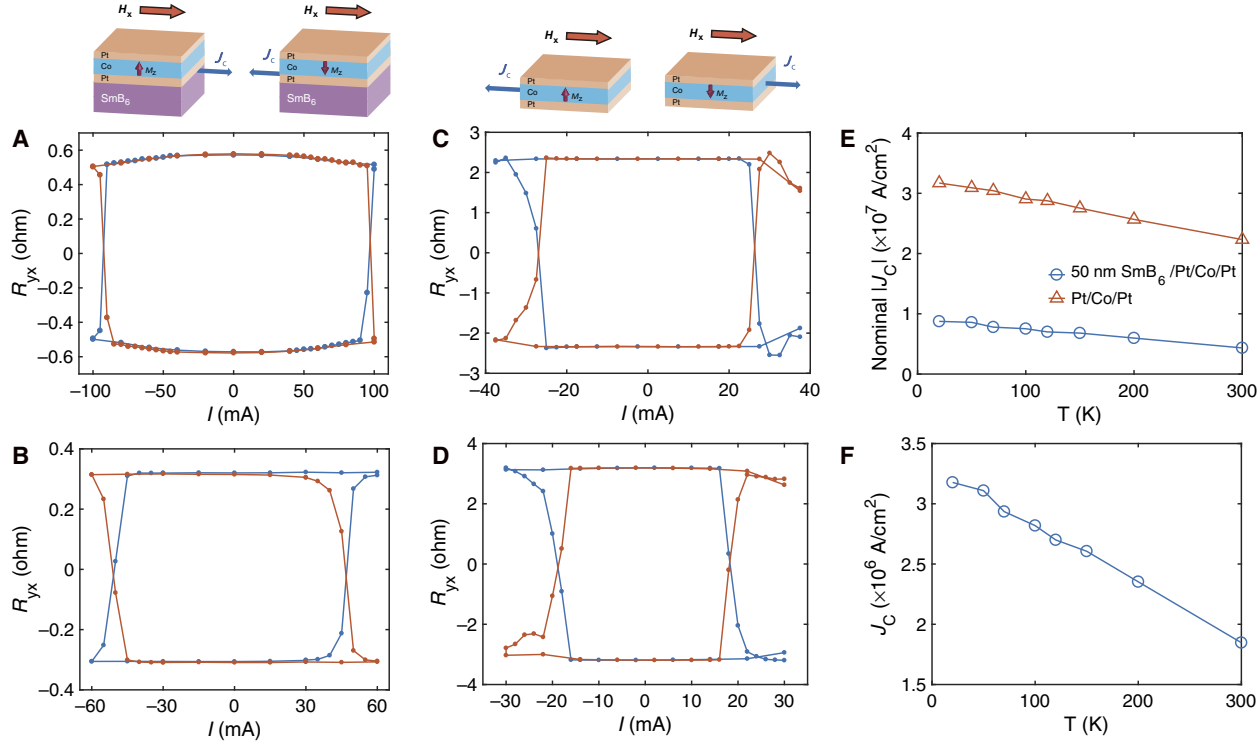

Fig. 5. SOT-induced switching of Pt/Co/Pt/SmB_6 devices. (**A** and **B**) SOT switching for Pt(1.7)/Co(0.5)/Pt(2)/SmB_6(50) measured at 20 K (A) and 300 K (B), with external magnetic fields 300 Oe (blue) and −300 Oe (red) applied along the *x* direction. (**C** and **D**) SOT switching for Pt(1.7)/Co(0.5)/Pt(2) measured at 20 K (C) and 300 K (D), with external magnetic fields of 300 Oe (blue) and −300 Oe (red) applied along the *x* direction. (**E**) Nominal critical current density of Pt(1.7)/Co(0.5)/Pt(2)/SmB_6(50) (blue) and Pt(1.7)/Co(0.5)/Pt(2) (red) multilayer films, where $|J_c|$ is calculated by dividing the total current by the thickness of the multilayer film. The external in-plane field is 300 Oe. (**F**) Critical current density required for SmB_6(50) that produces enough SOT to switch the Pt/Co/Pt PMA layer, under an in-plane field (H_x) of 300 Oe.

DISCUSSION

Here, we discuss our experimental results and their implications, in light of the proposed topological nature of SmB_6. Despite the observations in bulk crystals in the 100-μm range, the lack of 2D electrical transport feature in our thin films, with geometry dimensions controlled at a much higher precision, and most importantly on the 10-nm scale, poses challenge to the current understanding of SmB_6. Apparently, any possible scenarios that could reconcile the experimental observations in bulk and epitaxial thin films inevitably point toward extraordinary novel physical properties. One of the possibilities is that the surface state may reside on the boundaries of the crystalline domains within the thin films, which will introduce conduction channels in the bulk of the films that have the same temperature dependence as the presumed surface state but show thickness dependence. However, we must note that the opposite is believed to be true for TIs such as Bi_2Se_3 because scanning tunneling spectroscopy studies find that the grain boundaries do not host the surface state (*42*). Another possibility is that in SmB_6, the surface state may penetrate into a much greater depth, in sharp contrast with bismuth chalcogenide TIs, in which it is well established that the penetration depth is within several nanometers. However, given the much narrower band gap of SmB_6 (one to two orders of magnitude smaller than that of Bi_2Se_3), this suggests a likely explanation but invites further theoretical and experimental investigations.

Nevertheless, we have shown that SmB_6 is a source of strong SOT that can switch a room temperature FM layer. This unambiguously points to strong SOC, which is a key ingredient inherent to the formation of TIs. It is tempting to interpret the SOT as originating from the TSS. An electrical current flowing in the TSS is expected to induce spin accumulation due to the spin-momentum locking, which could be a source of pure spin current that gives rise to SOT. In Bi_2Se_3, the current-induced spin accumulation is found to be of little temperature dependence (*6*), which is similar to the SmB_6-contributed SOT observed in this work. However, in SmB_6, the hybridization gap between which the TSS resides only opens at temperatures below 100 to 150 K. Therefore, strong temperature dependence may be expected if the SOT originates from the presumed TSS of SmB_6, in contrast to the experimental observation. We tend to attribute the observed SOT to alternative origins, that is, the bulk spin Hall effect or the interfacial Rashba effect, which expects no marked temperature dependence. The monotonic enhancement of current-SOT conversion efficiency as the SmB_6 film thickness increases from 20 to 50 nm further suggests that the SOT most likely originates from the bulk spin Hall effect. The marked enhancement for films as thick as 50 nm indicates that the spin diffusion length in SmB_6 should be on the same scale, which is unusually long compared to those in HMs (usually only several nanometers).

In summary, despite many suggestions from bulk crystals that SmB_6 is a TKI with an insulating interior and a metallic conducting surface, SmB_6 thin films in the range of 10 to 100 nm do not reveal exclusive surface conduction state. However, SmB_6 thin films provide strong SOT, with a high current-SOT conversion efficiency comparable to β-W, the known HM with the largest spin Hall angle. The strong SOT hosted in SmB_6 may find its usefulness in spintronics.

METHODS

The SmB_6 thin films were synthesized by dc magnetron sputtering from a 99.9% pure SmB_6 target (Super Conductor Materials Inc.). The details of the film growth are as described in the main text. The MgO/CFB/W trilayer was deposited onto SmB_6/Si by dc and radio frequency magnetron sputtering at room temperature. The W layer was deposited at a low deposition rate of 0.3 nm/min to acquire the β phase, which was confirmed by its high bulk resistivity of >200 microhm·cm. A protective layer of 1-nm-thick Ta was capped on top of the trilayer to prevent it from oxidization. Control samples of the trilayer were grown on thermally oxidized silicon wafer. The trilayers with or without SmB_6 were subsequently annealed at 300°C in vacuum for 20 min to obtain PMA. The Pt/Co/Pt PMA trilayers were deposited onto SmB_6/Si(001) as well as thermally oxidized silicon substrate. The Pt/Co/Pt trilayers were prepared as-grown, without any post-annealing. The multilayer films were patterned into Hall bar devices with a width of 20 μm by standard ultraviolet lithography followed by Ar^+ milling. The electrical transport measurements were performed using Keithley 6221 current source and 2182A nanovoltmeter. For SOT-induced switching, a train of 50 switching current pulses was first applied (with a pulse width of 12 ms and a duty cycle of 10%) and then followed by a small dc probing current of 0.5 mA to measure the Hall effect.

SUPPLEMENTARY MATERIALS

Supplementary material for this article is available at http://advances.sciencemag.org/cgi/content/full/4/1/eaap8294/DC1

section S1. Comparison of the transport properties of SmB_6 thin films and single-crystal bulk specimens
section S2. Magnetoresistance and Hall effect
section S3. Additional data on crystalline and chemical stoichiometry characterizations
section S4. SOT-induced switching of perpendicularly magnetized CoFeB
section S5. Current distribution in multilayer thin films
fig. S1. Resistance ratio as a function of sample thicknesses.
fig. S2. Magnetoresistance of SmB_6 thin films.
fig. S3. Hall resistance of SmB_6 thin films.
fig. S4. Additional XRD data of SmB_6 thin films.
fig. S5. XPS spectrum of SmB_6 thin films.
fig. S6. Additional SOT switching results of various temperatures.
fig. S7. A schematic diagram of the anomalous Hall voltage measurement under the presence of a nonmagnetic shunting layer.
fig. S8. Temperature dependence of resistance of SmB_6 and CoFeB/W multilayers.
fig. S9. Sheet resistance of CoFeB/W multilayer as a function of W thicknesses.
References (*43*, *44*)

REFERENCES AND NOTES

1. M. Z. Hasan, C. L. Kane, *Colloquium*: Topological insulators. *Rev. Mod. Phys.* **82**, 3045–3067 (2010).
2. D. Kong, Y. Cui, Opportunities in chemistry and materials science for topological insulators and their nanostructures. *Nat. Chem.* **3**, 845–849 (2011).
3. A. R. Mellnik, J. S. Lee, A. Richardella, J. L. Grab, P. J. Mintun, M. H. Fischer, A. Vaezi, A. Manchon, E.-A. Kim, N. Samarth, D. C. Ralph, Spin-transfer torque generated by a topological insulator. *Nature* **511**, 449–451 (2014).
4. C. H. Li, O. M. J. van 't Erve, J. T. Robinson, Y. Liu, L. Li, B. T. Jonker, Electrical detection of charge-current-induced spin polarization due to spin-momentum locking in Bi_2Se_3. *Nat. Nanotechnol.* **9**, 218–224 (2014).
5. J. Tang, L.-T. Chang, X. Kou, K. Murata, E. S. Choi, M. Lang, Y. Fan, Y. Jiang, M. Montazeri, W. Jiang, Y. Wang, L. He, K. L. Wang, Electrical detection of spin-polarized surface states conduction in $(Bi_{0.53}Sb_{0.47})_2Te_3$ topological insulator. *Nano Lett.* **14**, 5423–5429 (2014).
6. A. Dankert, J. Geurs, M. V. Kamalakar, S. Charpentier, S. P. Dash, Room temperature electrical detection of spin polarized currents in topological insulators. *Nano Lett.* **15**, 7976–7981 (2015).
7. I. M. Miron, K. Garello, G. Gaudin, P.-J. Zermatten, M. V. Costache, S. Auffret, S. Bandiera, B. Rodmacq, A. S. P. Gambardella, Perpendicular switching of a single ferromagnetic layer induced by in-plane current injection. *Nature* **476**, 189–193 (2011).
8. L. Liu, O. J. Lee, T. J. Gudmundsen, D. C. Ralph, R. A. Buhrman, Current-induced switching of perpendicularly magnetized magnetic layers using spin torque from the spin Hall effect. *Phys. Rev. Lett.* **109**, 096602 (2012).
9. Y. Fan, P. Upadhyaya, X. Kou, M. Lang, S. Takei, Z. Wang, J. Tang, L. He, L.-T. Chang, M. Montazeri, G. Yu, W. Jiang, T. Nie, R. N. Schwartz, Y. Tserkovnyak, K. L. Wang,

Magnetization switching through giant spin–orbit torque in a magnetically doped topological insulator heterostructure. *Nat. Mater.* **13**, 699–704 (2014).
10. J. Han, A. Richardella, S. A. Siddiqui, J. Finley, N. Samarth, L. Liu, Room-temperature spin-orbit torque switching induced by a topological insulator. *Phys. Rev. Lett.* **119**, 077702 (2017).
11. D. C. Mahendra, M. Jamali, J.-Y. Chen, D. R. Hickey, D. Zhang, Z. Zhao, H. Li, P. Quarterman, Y. Lv, M. Li, K. A. Mkhoyan, J.-P. Wang, Room-temperature perpendicular magnetization switching through giant spin-orbit torque from sputtered BixSe(1-x) topological insulator material. http://arxiv.org/abs/1703.03822 (2017).
12. M. Dzero, K. Sun, V. Galitski, P. Coleman, Topological Kondo insulators. *Phys. Rev. Lett.* **104**, 106408 (2010).
13. M. Dzero, K. Sun, P. Coleman, V. Galitski, Theory of topological Kondo insulators. *Phys. Rev. B* **85**, 045130 (2012).
14. T. Takimoto, SmB_6: A promising candidate for a topological insulator. *J. Phys. Soc. Jpn.* **80**, 123710 (2011).
15. V. Alexandrov, M. Dzero, P. Coleman, Cubic topological Kondo insulators. *Phys. Rev. Lett.* **111**, 226403 (2013).
16. F. Lu, J. Zhao, H. Weng, Z. Fang, X. Dai, Correlated topological insulators with mixed valence. *Phys. Rev. Lett.* **110**, 096401 (2013).
17. J. C. Nickerson, R. M. White, K. N. Lee, R. Bachmann, T. H. Geballe, G. W. Hull Jr., Physical properties of SmB_6. *Phys. Rev. B* **3**, 2030–2042 (1971).
18. J. W. Allen, B. Batlogg, P. Wachter, Large low-temperature Hall effect and resistivity in mixed-valent SmB_6. *Phys. Rev. B* **20**, 4807–4813 (1979).
19. S. Wolgast, Ç. Kurdak, K. Sun, J. W. Allen, D.-J. Kim, Z. Fisk, Low-temperature surface conduction in the Kondo insulator SmB_6. *Phys. Rev. B* **88**, 180405 (2013).
20. D. J. Kim, S. Thomas, T. Grant, J. Botimer, Z. Fisk, J. Xia, Surface Hall effect and nonlocal transport in SmB_6: Evidence for surface conduction. *Sci. Rep.* **3**, 3150 (2013).
21. D. J. Kim, J. Xia, Z. Fisk, Topological surface state in the Kondo insulator samarium hexaboride. *Nat. Mater.* **13**, 466–470 (2014).
22. Y. Xu, I. Miotkowski, C. Liu, J. Tian, H. Nam, N. Alidoust, J. Hu, C.-K. Shih, M. Z. Hasan, Y. P. Chen, Observation of topological surface state quantum Hall effect in an intrinsic three-dimensional topological insulator. http://arxiv.org/abs/1409.3778 (2014).
23. R. Yoshimi, A. Tsukazaki, Y. Kozuka, J. Falson, K. S. Takahashi, J. G. Checkelsky, N. Nagaosa, M. Kawasaki, Y. Tokura, Quantum Hall effect on top and bottom surface states of topological insulator $(Bi_{1-x}Sb_x)_2Te_3$ films. *Nat. Commun.* **6**, 6627 (2015).
24. N. Xu, X. Shi, P. K. Biswas, C. E. Matt, R. S. Dhaka, Y. Huang, N. C. Plumb, M. Radovic, J. H. Dil, E. Pomjakushina, K. Conder, A. Amato, Z. Salman, D. McK. Paul, J. Mesot, H. Ding, M. Shi, Surface and bulk electronic structure of the strongly correlated system SmB6 and implications for a topological Kondo insulator. *Phys. Rev. B* **88**, 121102 (2013).
25. J. Jiang, S. Li, T. Zhang, Z. Sun, F. Chen, Z. R. Ye, M. Xu, Q. Q. Ge, S. Y. Tan, X. H. Niu, M. Xia, B. P. Xie, Y. F. Li, X. H. Chen, H. H. Wen, D. L. Feng, Observation of possible topological in-gap surface states in the Kondo insulator SmB6 by photoemission. *Nat. Commun.* **4**, 3010 (2013).
26. M. Neupane, N. Alidoust, S.-Y. Xu, T. Kondo, Y. Ishida, D. J. Kim, C. Liu, I. Belopolski, Y. J. Jo, T.-R. Chang, H.-T. Jeng, T. Durakiewicz, L. Balicas, H. Lin, A. Bansil, S. Shin, Z. Fisk, M. Z. Hasan, Surface electronic structure of the topological Kondo-insulator candidate correlated electron system SmB_6. *Nat. Commun.* **4**, 2991 (2013).
27. Z.-H. Zhu, A. Nicolaou, G. Levy, N. P. Butch, P. Syers, X. F. Wang, J. Paglione, G. A. Sawatzky, I. S. Elfimov, A. Damascelli, Polarity-driven surface metallicity in SmB_6. *Phys. Rev. Lett.* **111**, 216402 (2013).
28. E. Frantzeskakis, N. de Jong, B. Zwartsenberg, Y. K. Huang, Y. Pan, X. Zhang, J. X. Zhang, F. X. Zhang, L. H. Bao, O. Tegus, A. Varykhalov, A. de Visser, M. S. Golden, Kondo hybridization and the origin of metallic states at the (001) surface of SmB_6. *Phys. Rev. X* **3**, 041024 (2013).
29. N. Xu, P. K. Biswas, J. H. Dil, R. S. Dhaka, G. Landolt, S. Muff, C. E. Matt, X. Shi, N. C. Plumb, M. Radović, E. Pomjakushina, K. Conder, A. Amato, S. V. Borisenko, R. Yu, H.-M. Weng, Z. Fang, X. Dai, J. Mesot, H. Ding, M. Shi, Direct observation of the spin texture in SmB_6 as evidence of the topological Kondo insulator. *Nat. Commun.* **5**, 4566 (2014).
30. P. Hlawenka, K. Siemensmeyer, E. Weschke, A. Varykhalov, J. Sánchez-Barriga, N. Y. Shitsevalova, A. V. Dukhnenko, V. B. Filipov, S. Gabáni, K. Flachbart, O. Rader, E. D. L. Rienks, Samarium hexaboride: A trivial surface conductor. http://arxiv.org/abs/1502.01542 (2015).
31. G. Li, Z. Xiang, F. Yu, T. Asaba, B. Lawson, P. Cai, C. Tinsman, A. Berkley, S. Wolgast, Y. S. Eo, D.-J. Kim, C. Kurdak, J. W. Allen, K. Sun, X. H. Chen, Y. Y. Wang, Z. Fisk, L. Li, Two-dimensional Fermi surfaces in Kondo insulator SmB_6. *Science* **346**, 1208–1212 (2014).
32. B. S. Tan, Y.-T. Hsu, B. Zeng, M. Ciomaga Hatnean, N. Harrison, Z. Zhu, M. Hartstein, M. Kiourlappou, A. Srivastava, M. D. Johannes, T. P. Murphy, J.-H. Park, L. Balicas, G. G. Lonzarich, G. Balakrishnan, S. E. Sebastian, Unconventional Fermi surface in an insulating state. *Science* **349**, 287–290 (2015).
33. S. Rößler, T.-H. Jang, D.-J. Kim, L. H. Tjeng, Z. Fisk, F. Steglich, S. Wirth, Hybridization gap and Fano resonance in SmB_6. *Proc. Natl. Acad. Sci. U.S.A.* **111**, 4798–4802 (2014).
34. W. A. Phelan, S. M. Koohpayeh, P. Cottingham, J. W. Freeland, J. C. Leiner, C. L. Broholm, T. M. McQueen, Correlation between bulk thermodynamic measurements and the low-temperature-resistance plateau in SmB_6. *Phys. Rev. X* **4**, 031012 (2014).
35. P. Syers, D. Kim, M. S. Fuhrer, J. Paglione, Tuning bulk and surface conduction in the proposed topological Kondo insulator SmB6. *Phys. Rev. Lett.* **114**, 096601 (2015).
36. W. Waldhauser, C. Mitterer, J. Laimer, H. Störi, Sputtered thermionic hexaboride coatings. *Surf. Coat. Technol.* **98**, 1315–1323 (1998).
37. J. Yong, Y. Jiang, D. Usanmaz, S. Curtarolo, X. Zhang, L. Li, X. Pan, J. Shin, I. Takeuchi, R. L. Greene, Robust topological surface state in Kondo insulator SmB_6 thin films. *Appl. Phys. Lett.* **105**, 222403 (2014).
38. N. Wakeham, Y. Q. Wang, Z. Fisk, F. Ronning, J. D. Thompson, Surface state reconstruction in ion-damaged SmB_6. *Phys. Rev. B* **91**, 085107 (2015).
39. Q. Hao, G. Xiao, Giant spin Hall effect and switching induced by spin-transfer torque in a $W/Co_{40}Fe_{40}B_{20}/MgO$ structure with perpendicular magnetic anisotropy. *Phys. Rev. Appl.* **3**, 034009 (2015).
40. C.-F. Pai, L. Liu, Y. Li, H. W. Tseng, D. C. Ralph, R. A. Buhrman, Spin transfer torque devices utilizing the giant spin Hall effect of tungsten. *Appl. Phys. Lett.* **101**, 122404 (2012).
41. D. Qu, S. Y. Huang, B. F. Miao, S. X. Huang, C. L. Chien, Self-consistent determination of spin Hall angles in selected 5*d* metals by thermal spin injection. *Phys. Rev. B* **89**, 140407 (2014).
42. Y. Liu, Y. Y. Li, D. Gilks, V. K. Lazarov, M. Weinert, L. Li, Charging Dirac states at antiphase domain boundaries in the three-dimensional topological insulator Bi_2Se_3. *Phys. Rev. Lett.* **110**, 186804 (2013).
43. N. E. Sluchanko, V. V. Glushkov, S. V. Demishev, A. A. Pronin, A. A. Volkov, M. V. Kondrin, A. K. Savchenko, S. Kunii, , Low-temperature transport anisotropy and many-body effects in SmB_6. *Phys. Rev. B* **64**, 153103 (2001).
44. J. Yong, Y. Jiang, X. Zhang, J. Shin, I. Takeuchi, R. L. Greene, Magnetotransport in nanocrystalline SmB_6 thin films. *AIP Adv.* **5**, 077144 (2015).

Acknowledgments: We thank A. H. Macdonald, A. Turner, T. M. McQueen, and W. A. Phelan for fruitful discussions. **Funding:** This work was supported in part by Sustainable and Holistic Integration of Energy Storage and Solar Photovoltaics (SHINES), grant SC0012670, the Energy Frontier Research Center of U.S. Department of Energy, and grant DE-SC0009390. Q.M. was supported in part by STARnet, a Semiconductor Research Corporation (SRC) program sponsored by Microelectronics Advanced Research Corporation (MARCO) and Defense Advanced Research Projects Agency (DARPA), under contract 2013-MA-2831. **Author contributions:** Y.L. and C.L.C. conceived the project. Y.L. prepared the SmB_6 films with the help of S.X.H. Q.M. and Y.L. prepared the PMA layers. Y.L. performed the measurements and analyzed the data. Y.L. and C.L.C. wrote the manuscript, and all authors discussed the result and commented on the manuscript. **Competing interests:** Y.L., Q.M., and C.L.C. are authors on a patent application filed through Johns Hopkins University that relates to this work (application no. 15/497,591; filed 26 April 2017). C.L.C. declares that he has no competing interests. **Data and materials availability:** All data needed to evaluate the conclusions in the paper are present in the paper and/or the Supplementary Materials. Additional data related to this paper may be requested from the authors.

Submitted 31 August 2017
Accepted 14 December 2017
Published 19 January 2018
10.1126/sciadv.aap8294

Citation: Y. Li, Q. Ma, S. X. Huang, C. L. Chien, Thin films of topological Kondo insulator candidate SmB_6: Strong spin-orbit torque without exclusive surface conduction. *Sci. Adv.* **4**, eaap8294 (2018).